188 *Inorg. Chem.* **2010**, *49*, 188–198
DOI: 10.1021/ic9017272

Inorganic Chemistry
Article

Density Functional Theory Applied to a Difference in Pathways Taken by the Enzymes Cytochrome P450 and Superoxide Reductase: Spin States of Ferric Hydroperoxo Intermediates and Hydrogen Bonds from Water

Panida Surawatanawong, Jesse W. Tye, and Michael B. Hall*

Department of Chemistry, Texas A&M University, College Station, Texas 77843-3255

Received August 31, 2009

Cytochrome P450 monooxygenase and superoxide reductase (SOR) have the same first atom coordination shell at their iron active sites: an Fe[N_4S] center in a square-pyramidal geometry with the sixth coordinate site open for the catalytic reaction. Furthermore, both pass through ferric hydroperoxo intermediates. Despite these similarities, the next step in their catalytic cycle is very different: distal oxygen protonation and O−O cleavage (P450) versus proximal oxygen protonation and H_2O_2 release (SOR). One of the factors leading to this difference is the spin state of the intermediates. Density functional theory (DFT) applied to models for the ferric hydroperoxo, $(SCH_3)(L)Fe^{III}-OOH$ (L = porphyrin for P450 and four imidazoles for SOR), gives different ground spin states; the P450 model with the porphyrin, which contrains the Fe−N distances, prefers a low-spin ground state, whereas the SOR model with four histidines, in which Fe−N bonds are extendable, prefers a high-spin ground state. Their ground spin states lead to geometric and electronic structures that assist in (1) the protonation on distal oxygen for P450, which leads to O−O bond cleavage and formation of the oxo-ferryl, $(SCH_3)(L)Fe^{IV}=O$ (Cpd I), and H_2O, and (2) the protonation on proximal oxygen for SOR, which leads to the formation of the ferric hydrogen peroxide, $(SCH_3)(L)Fe^{III}-HOOH$, intermediate before the Fe−O bond cleavage and H_2O_2 production. Specifically, the quartet ground state of the water-bound oxo-ferryl, $(SCH_3)(L)Fe^{IV}=O\cdots H_2O$, is more stable than the sextet ground state of $(SCH_3)(L)Fe^{III}-HOOH$ by −14.29 kcal/mol for the P450 model. Another important factor is the differences in the location of the active site: P450's active site is embedded within the enzyme, whereas SOR's active site is exposed to the aqueous environment. In the latter location, water molecules can freely form hydrogen bonds with both proximal and distal oxygen to stabilize the $(SCH_3)(L)Fe^{III}-HOOH$ intermediate. When two explicit water molecules are included in the model, the sextet ground state of $(SCH_3)(L)Fe^{III}-HOOH\cdots 2H_2O$ is more stable than the quartet ground state of $(SCH_3)(L)Fe^{IV}=O\cdots 3H_2O$ by −2.14 kcal/mol for the SOR model. Our calculations show that both the spin state, which is controlled by the differences between four N donors in porphyrin versus those in imidazoles, and the degree of solvent exposure of the active sites play important roles in the fate of the $(SCH_3)(L)Fe^{III}-OOH$ intermediate, leading to O−O cleavage in one situation (P450) and hydrogen peroxide production in the other (SOR).

Introduction

The active sites of both superoxide reductase (SOR) and cytochrome P450 monooxygenase enzymes have the same first coordination sphere containing an iron center coordinated by four nitrogen donor atoms and one cysteinate sulfur in a square-pyramidal arrangement (Fe[N_4S] center). However, these enzymes catalyze very different reactions.[1−3] Superoxide reductase is a non-heme iron enzyme for detoxification of superoxide in anaerobic organisms.[4−6] The histidine and cysteine ligated iron active site of SOR binds superoxide, catalyzes one-electron reduction, and produces hydrogen peroxide (i.e., $O_2^- + 2H^+ + e^- \rightarrow H_2O_2$). The cytochrome P450 monooxygenase is a heme iron enzyme for biosynthesis of steroids, detoxification of xenobiotics, and metabolism of drugs.[7,8] The porphyrin and cysteine ligated iron active site of P450 binds O_2 and catalyzes two-electron reduction and double protonation of O_2 to cleave the O−O bond to yield one equivalent of H_2O and the high valent iron−oxo complex, known as Compound I (Cpd I), that catalyzes the stereospecific alkane hydroxylation reactions.

*To whom correspondence should be addressed. E-mail: mbhall@tamu.edu.

(1) Kovacs, J. A. *Chem. Rev.* **2004**, *104*, 825–848.
(2) Kovacs, J. A.; Brines, L. M. *Acc. Chem. Res.* **2007**, *40*, 501–509.
(3) Kovacs, J. A. *Science* **2003**, *299*, 1024–1025.
(4) Francis E. Jenney, J.; Verhagen, M. F. J. M.; Cui, X.; Adams, M. W. W. *Science* **1999**, *286*, 306–309.
(5) Lombard, M.; Fontecave, M.; Touati, D.; Nivière, V. *J. Biol. Chem.* **2000**, *275*, 115–121.
(6) Imlay, J. A. *J. Biol. Inorg. Chem.* **2002**, *7*, 659–663.
(7) Sono, M.; Roach, M. P.; Coulter, E. D.; Dawson, J. H. *Chem. Rev.* **1996**, *96*, 2841–2887.
(8) Denisov, I. G.; Makris, T. M.; Sligar, S. G.; Schlichting, I. *Chem. Rev.* **2005**, *105*, 2253–2277.

 Published on Web 12/07/2009 © 2009 American Chemical Society

Scheme 1. Catalytic Cycle of SOR and P450

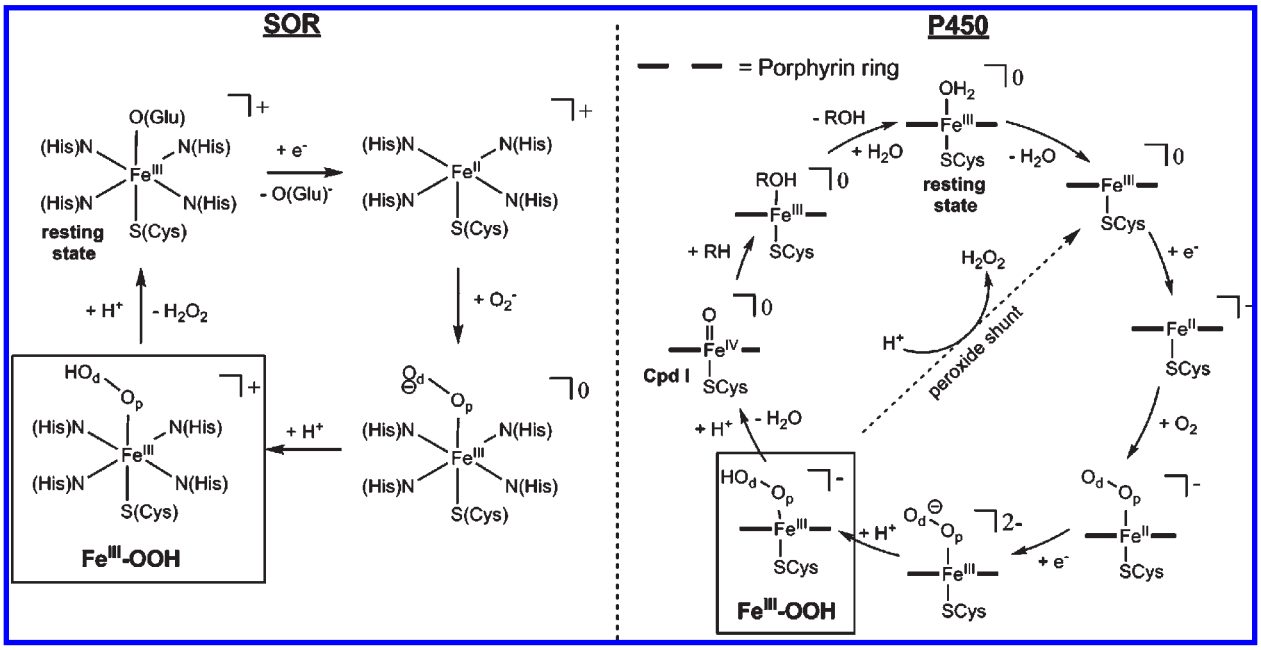

The generally accepted catalytic mechanisms for P450[7,8] and SOR[9−11] are compared in Scheme 1. In both SOR and P450 mechanisms, after one-electron reduction of the ferric (Fe^{III}) resting state, a dioxygen species (O_2^- and O_2, respectively) binds to the ferrous (Fe^{II}) center with the addition of one electron to the P450 yielding a ferric peroxo ($Fe^{III}-OO$) intermediate for both. Protonation of the distal oxygen (terminal oxygen), O_d, yields a ferric hydroperoxo ($Fe^{III}-OOH$) species, a common intermediate in both enzymes.[1] However, this common intermediate proceeds through two very different reactions. A second protonation on the proximal oxygen (iron-bound oxygen), O_p, leads to the formation and release of hydrogen peroxide (HOOH), the product of SOR. The production of hydrogen peroxide is also a side reaction for P450 (also known as an uncoupling or decoupling reaction since it wastes reducing equivalents and O_2).[12] On the other hand, the productive reaction in P450 involves a second protonation on the distal oxygen that leads to loss of H_2O and formation of an oxo-ferryl ($Fe^{IV}=O$) species (Cpd I).

The SOR and P450 enzymes also differ significantly in the location of the enzyme active sites within their respective proteins. The P450 enzyme active site is located inside an enclosed pocket that is buried in the protein. Well-defined O_2 and alkane access channels, which also serve as H_2O and product egress channels, connect the P450 enzyme active site to the protein surface.[13] Similarly, well-defined hydrogen-bonded proton-transfer pathways deliver protons from the protein surface to the P450 enzyme active site.[13,14] In marked constrast, the active site of SOR is located in a cavity on the surface of the SOR enzyme that is fully exposed to water molecules.[10,15]

Recent computational studies have provided new insights into the formation of an oxo-ferryl complex in P450 and the production of hydrogen peroxide in SOR. The protonation of $Fe^{III}-OOH$ at the distal oxygen is found to be more favorable than the protonation at the proximal oxygen from several theoretical studies of P450 models.[16−18] Later DFT and QM/MM studies also show that the water network shuttles the proton from nearby amino acid residues to protonate the distal oxygen of $Fe^{III}-OOH$ in P450 models.[19−23] The role of a water molecule to stabilize the oxo-ferryl complex in hydroxylation by P450 has also been studied.[24,25] For one SOR model, the formation of hydrogen peroxide has been investigated computationally. Kurtz and co-workers performed density functional calculation on various mono- and diprotonated peroxo ferric SOR model complexes and found that the protonation at the proximal oxygen is an important step to the decay of $Fe^{III}-OOH$ and release of hydrogen peroxide.[26]

(9) Adams, M. W. W.; Jenney, F. E., Jr.; Clay, M. D.; Johnson, M. K. *J. Biol. Inorg. Chem.* **2002**, *7*, 647–652.
(10) Kurtz, D. M., Jr. *Acc. Chem. Res.* **2004**, *37*, 902–908.
(11) Kurtz, D. M., Jr.; Coulter, E. D. *J. Biol. Inorg. Chem.* **2002**, *7*, 653–658.
(12) Imai, M.; Shimada, H.; Watanabe, Y.; Matsushima-Hibaya, Y.; Makino, R.; Koga, H.; Horiuchi, T.; Ishimura, Y. *Proc. Natl. Acad. Sci. U.S.A.* **1989**, *86*, 7823–7827.
(13) Schlichting, I.; Berendzen, J.; Chu, K.; Stock, A. M.; Maves, S. A.; Benson, D. E.; Sweet, R. M.; Ringe, D.; Petsko, G. A.; Sligar, S. G. *Science* **2000**, *287*, 1615–1622.
(14) Shaik, S.; Kumar, D.; de Visser, S. P.; Altun, A.; Thiel, W. *Chem. Rev.* **2005**, *105*, 2279–2328.
(15) Yeh, A. P.; Hu, Y.; Francis, E.; Jenney, J.; Adams, M. W. W.; Rees, D. C. *Biochemistry* **2000**, *39*, 2499–2508.
(16) Harris, D. L.; Loew, G. H. *J. Am. Chem. Soc.* **1998**, *120*, 8941–8948.
(17) Hata, M.; Hirano, Y.; Hoshino, T.; Nishida, R.; Tsuda, M. *J. Phys. Chem. B* **2004**, *108*, 11189–11195.
(18) Bach, R. D.; Dmitrenko, O. *J. Am. Chem. Soc.* **2006**, *128*, 1474–1488.
(19) Guallar, V.; Friesner, R. A. *J. Am. Chem. Soc.* **2004**, *126*, 8501–8508.
(20) Kumar, D.; Hirao, H.; de Visser, S. P.; Zheng, J.; Wang, D.; Thiel, W.; Shaik, S. *J. Phys. Chem. B* **2005**, *109*, 19946–19951.
(21) Zheng, J.; Wang, D.; Thiel, W.; Shaik, S. *J. Am. Chem. Soc.* **2006**, *128*, 13204–13215.
(22) Kamachi, T.; Yoshizawa, K. *J. Am. Chem. Soc.* **2003**, *125*, 4652–4661.
(23) Altarsha, M.; Benighaus, T.; Kumar, D.; Thiel, W. *J. Am. Chem. Soc.* **2009**, *131*, 4755–4763.
(24) Altun, A.; Guallar, V.; Friesner, R. A.; Shaik, S.; Thiel, W. *J. Am. Chem. Soc.* **2006**, *128*, 3924–3925.
(25) Altun, A.; Shaik, S.; Thiel, W. *J. Comput. Chem.* **2006**, *27*, 1324–1337.
(26) Silaghi-Dumitrescu, R.; Silaghi-Dumitrescu, I.; Coulter, E. D.; Kurtz, D. M. *J. Inorg. Chem.* **2003**, *42*, 446–456.

Relatively few computational and spectroscopic studies have been done for the structures and reactivity of the intermediates in the SOR active site in comparison to the corresponding ones in the P450 active site.[27,28] Yang et al. studied the electronic properties of cyano-ferric intermediates for both enzymes by ENDOR measurements complemented with DFT calculation and found that the difference in the in-plane heme and out-of-plane dihedral of four histidines and the inclusion of H bonds to the cysteine axial ligands cause different spin density distribution on sulfur in the active sites.[27] Solomon and co-workers suggested that the strong equatorial ligand field from the porphyrin results in a low-spin $Fe^{III}-OOH$, which will not support the H_2O_2 release because of the spin-crossing barrier in the formation of the high-spin ferric pentacoordinate product; in contrast, the dianionic porphyrin could assist the formation of the oxo-ferryl complex.[28]

Still missing was a careful comparison of the $Fe^{III}-OOH$ structures in all possible spin states for SOR and P450 models that may explain how the high-spin structure supports Fe−O bond cleavage and low-spin structure supports O−O bond cleavage. Moreover, the effect from the difference in the iron active site location (environment) in these two enzymes had not been carefully compared. Therefore, a comparison of both reactions for models of both active sites is presented in detail here. To understand the factors leading to the difference in the reaction pathways between these two similar active site enzymes, the structural properties of the corresponding model intermediates from both enzymes will be compared, including the effects from different active site locations, which have not been addressed elsewhere. Here, we used density functional theory (DFT) calculation to study the geometric parameters, electronic structures, and relative free energies of possible spin states for the model of ferric hydroperoxo, $(SCH_3)(L)Fe^{III}-OOH$ (L = four imidazoles for SOR and porphyrin for P450), the common intermediate of SOR and P450, to examine the factors leading to key differences in the next step for both enzyme models. Then, the formation of ferric hydrogen peroxide complex, $(SCH_3)(L)Fe^{III}-HOOH$, is compared to the formation of oxo-ferryl complex, $(SCH_3)(L)Fe^{IV}=O$, for both enzyme active site models. Finally, we studied the effect from the solvent-exposed position of the active site in SOR enzymes to the production of hydrogen peroxide by including explicit water molecules in the calculation of the $(SCH_3)(L)Fe^{III}-HOOH$ intermediate.

Computational Details

In both iron active site models (SOR and P450), a methyl thiolate (SCH_3^-) is used as the axial ligand. For the equatorial ligands, the four histidines in SOR are replaced by four neutral imidazole (ImH) ligands (Scheme 2) and the heme in P450 was replaced by porphyrin (Por) (Scheme 3). For all SOR models, the crystal structure in the resting ferric state with glutamate bound at the sixth coordinate (PDB code: 1DQI)[15] was used as the starting structure. The sixth coordinate ligand was replaced by acetate (CH_3COO^- or OAc^-) in

Scheme 2. $[(SCH_3)(ImH)_4Fe^{III}-OAc]^+$ Model for the SOR Active Site[a]

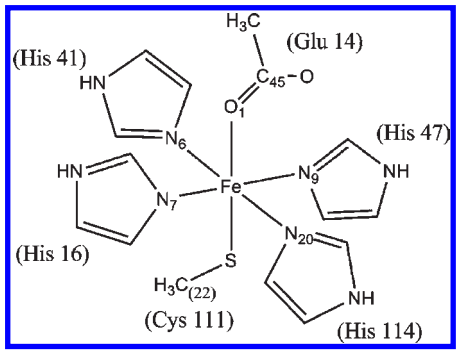

[a] The residue numbers in parentheses are from the crystal structure of the *Pyrococcus furiosus* SOR structure in ref 15.

Scheme 3. $(SCH_3)(Por)Fe^{III}-X$ model for P450 Active Site (X = OOH^-, HOOH, and O^{2-})

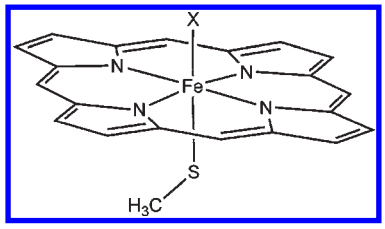

the model of glutamate-bound resting state, $[(SCH_3)(ImH)_4Fe^{III}-OAc]^+$, and by hydroperoxo ($OOH^-$), hydrogen peroxide (HOOH), and oxo (O^{2-}) in the models of ferric hydroperoxo $[(SCH_3)(ImH)_4Fe^{III}-OOH]^+$, ferric hydrogen peroxide $[(SCH_3)(ImH)_4Fe^{III}-HOOH]^{2+}$, and oxo-ferryl $[(SCH_3)(ImH)_4Fe^{IV}=O]^{2+}$ complexes, respectively. For all P450, the crystal structure of cytochrome P450 from PDB code 1DZ8[13] was used as the starting structure. As in the SOR models, the sixth coordinate was replaced by hydroperoxo, hydrogen peroxide, and oxo in the model of $[(SCH_3)(Por)Fe^{III}-OOH]^-$ (Por = porphyrin), $[(SCH_3)(Por)Fe^{III}-HOOH]^0$, and $[(SCH_3)(Por)Fe^{IV}=O]^0$ complexes, respectively. Note that we refer to the oxidation state of the iron in the oxo complex as Fe^{IV} for both SOR and P450 models because the spin density calculation suggested that there is a radical delocalized on the thiolate and the equatorial ligands (see later in the text).

All calculations were performed with the Gaussian03 program package.[29] The PBE[30] density functional was used for all geometry optimization with basis set I (BS-I), in which modified LANL2DZ+f basis set with effective core

(27) Yang, T.-C.; McNaughton, R. L.; Clay, M. D.; Francis E. Jenney, J.; Krishnan, R.; Kurtz, D. M.; Adams, M. W. W.; Johnson, M. K.; Hoffman, B. M. *J. Am. Chem. Soc.* **2006**, *128*, 16566–16578.

(28) Dey, A.; Francis E. Jenney, J.; Adams, M. W. W.; Johnson, M. K.; Hodgson, K. O.; Hedman, B.; Solomon, E. I. *J. Am. Chem. Soc.* **2007**, *129*, 12418–12431.

(29) Frisch, M. J.; Trucks, G. W.; Schlegel, H. B.; Scuseria, G. E.; Robb, M. A.; Cheeseman, J. R.; Montgomery, J. A., Jr.; Vreven, T.; Kudin, K. N.; Burant, J. C.; Millam, J. M.; Iyengar, S. S.; Tomasi, J.; Barone, V.; Mennucci, B.; Cossi, M.; Scalmani, G.; Rega, N.; Petersson, G. A.; Nakatsuji, H.; Hada, M.; Ehara, M.; Toyota, K.; Fukuda, R.; Hasegawa, J.; Ishida, M.; Nakajima, T.; Honda, Y.; Kitao, O.; Nakai, H.; Klene, M.; Li, X.; Knox, J. E.; Hratchian, H. P.; Cross, J. B.; Adamo, C.; Jaramillo, J.; Gomperts, R.; Stratmann, R. E.; Yazyev, O.; Austin, A. J.; Cammi, R.; Pomelli, C.; Ochterski, J. W.; Ayala, P. Y.; Morokuma, K.; Voth, G. A.; Salvador, P.; Dannenberg, J. J.; Zakrzewski, V. G.; Dapprich, S.; Daniels, A. D.; Strain, M. C.; Farkas, O.; Malick, D. K.; Rabuck, A. D.; Raghavachari, K.; Foresman, J. B.; Ortiz, J. V.; Cui, Q.; Baboul, A. G.; Clifford, S.; Cioslowski, J.; Stefanov, B. B.; Liu, G.; Liashenko, A.; Piskorz, P.; Komaromi, I.; Martin, R. L.; Fox, D. J.; Keith, T.; Al-Laham, M. A.; Peng, C. Y.; Nanayakkara, A.; Challacombe, M.; Gill, P. M. W.; Johnson, B.; Chen, W.; Wong, M. W.; Gonzalez, C.; Pople, J. A. *Gaussian 03*, revision B.4, B.5, and C.1; Gaussian, Inc.: Pittsburgh, PA, 2003.

(30) Perdew, J. P.; Burke, K.; Ernzerhof, M. *Phys. Rev. Lett.* **1996**, *77*, 3865–3868.

Table 1. Geometry Parameters and Relative Free Energies of $(SCH_3)(ImH)_4Fe^{III}-OAc$ for the SOR Model

	1DQI[a]	1DO6[a]	B3LYP//PBE/BS-II			B3LYP//PBE/BS-I			B3LYP/BS-I		
S	5/2	5/2	1/2	3/2	5/2	1/2	3/2	5/2	1/2	3/2	5/2
ΔG(PBE) (kcal/mol)			0.00	9.93	11.01	0.00	6.79	5.40			
ΔG(B3LYP) (kcal/mol)			0.00	−1.56	−8.39	0.00	−1.79	−8.84	0.00	−4.02	−8.60
			geometry (Å, deg)								
Fe−O1	2.15	2.01	1.99	1.95	2.00	2.01	1.93	2.01	2.00	1.97	2.02
Fe−S	2.46	2.42	2.21	2.23	2.37	2.23	2.28	2.41	2.28	2.34	2.40
Fe−N7	2.09	2.14	2.02	2.04	2.20	2.01	2.04	2.21	2.03	2.09	2.21
Fe−N20	2.20	2.09	1.99	2.34	2.22	2.01	2.37	2.24	2.05	2.33	2.24
Fe−N9	2.16	2.20	2.00	2.03	2.17	2.01	2.02	2.18	2.03	2.07	2.19
Fe−N6	2.20	2.15	1.97	2.28	2.21	1.97	2.35	2.23	2.00	2.30	2.22
Fe−S−C22	117.0	117.6	114.1	112.1	111.4	115.3	111.4	110.4	114.8	111.4	113.8
Fe−O1−C45	175.0	162.7	133.1	136.0	146.7	134.5	135.5	149.3	135.3	136.7	140.3
N7−Fe−S−C22	10.4	18.4	−7.8	8.7	−19.1	−34.9	10.1	−18.6	−39.9	8.4	−11.7

[a] PDB codes of the X-ray crystal structures from ref 15.

potentials (ECP)[31−33] is used for Fe; 6-31++G(d,p)[34−36] is used for sulfur, iron-bound nitrogen, and oxygen and hydrogen atoms of H_2O and H_2O_2; and 6-31G(d)[34−36] is used for all other atoms. Basis set II (BS-II) used 6-31++G(d,p) and basis set III (BS-III) used the Wachter's basis set for iron,[37] while the rest is identical to BS-I. Mulliken charges on Fe are negative for BS-I but positive for BS-III, but the trends are similar (see Supporting Information). The effect of the basis set on the geometry optimization was examined for BS-I and BS-II for the SOR model as $[(SCH_3)(ImH)_4Fe^{III}-OAc]^+$, the experimental structured active site. All structures were fully optimized, and frequency calculations were calculated to ensure that there were no imaginary frequencies for minima. Frequency calculations were performed with the PBE functional, and single-point energies were recalculated with the B3LYP functional[38,39] in the same basis set. Zero-point energies and thermodynamic functions were calculated at 298.15 K and 1 atm. Unless specified otherwise, the energies mentioned throughout the Article refer to the B3LYP relative free energies.

Results and Discussion

We begin with the density functional calculation of $[(SCH_3)(ImH)_4Fe^{III}-OAc]^+$, the model for ferric resting state of SOR, to compare geometry parameters and spin states with those from the crystal structures (PDB: 1DQI and 1DO6)[15] and spin state measurements.[40] Then, the electronic structures of all possible spin states for ferric hydroperoxo model, $(SCH_3)(L)Fe^{III}-OOH$, a common intermediate of SOR (L = ImH_4) and P450 (L = Por), will be examined for the factors which might lead to different pathways in each enzyme. The protonation at distal oxygen of $(SCH_3)(L)Fe^{III}-OOH$ leads to O−O bond cleavage and $(SCH_3)(L)Fe^{IV}=O$ and H_2O product formation (the main product for P450), whereas the protonation at proximal oxygen leads to $(SCH_3)(L)Fe^{III}-HOOH$ intermediates and Fe−O bond cleavage releasing hydrogen peroxide as a product (the product for SOR).[16] Therefore, the stability of $(SCH_3)(L)Fe^{III}-HOOH$ and $(SCH_3)(L)Fe^{IV}=O$ intermediates will be compared for both SOR and P450 models. Finally, to represent the degree of solvent exposure at the active site of the enzymes, we will also compare the stability of $(SCH_3)(L)Fe^{III}-HOOH$ and $(SCH_3)(L)Fe^{IV}=O$ complexes that include hydrogen bonds from explicit water molecules.

Ferric Acetate Model, $[(SCH_3)(ImH)_4Fe^{III}-OAc]^+$, the Resting State of SOR. The crystal structures of the iron active site in SOR show that the iron center binds to four histidine ligands at the equatorial plane and one cysteine at the axial position; the sixth coordinate is either found empty[41,42] or varies from glutamate,[15,43] water,[15] to (hydro)peroxide.[43] Typically, the water molecule binds loosely to the iron center (Fe−O ∼ 2.6 Å).[15] On the other hand, the glutamate binds tightly at the ferric resting state of SOR,[15] and in this form, the system is known to be in the high-spin ($S = 5/2$) state.[40] Therefore, we chose to perform geometry optimizations on all possible spin state ($S = 1/2$, 3/2, and 5/2) for $[(SCH_3)(ImH)_4Fe^{III}-OAc]^+$ (Scheme 2) to verify the accuracy of PBE and B3LYP density functionals for one of our model calculation systems in comparison to the glutamate-bound ferric resting state from the crystal structure.[15] The geometry parameters from calculations and the crystal structure are shown in Table 1, and atom labels are displayed in Scheme 2. The PBE relative free energies and structures from the "all-electron" basis set on iron (BS-II) can also be compared to those from an effective core potential (ECP) on iron (BS-I). The Fe−ligand atom bond distances are closest to the crystal structure for the high-spin state in both PBE and B3LYP optimization (Table 1). In particular, the Fe−N bonds are computed to be only slightly too long in the high-spin case but much too short in the low-spin case and much too varied in the intermediate-spin case. Therefore, the computed Fe−N distances of the high-spin

(31) Hay, P. J.; Wadt, W. R. *J. Chem. Phys.* **1985**, *82*, 270–283.
(32) Hay, P. J.; Wadt, W. R. *J. Chem. Phys.* **1985**, *82*, 299–310.
(33) Couty, M.; Hall, M. B. *J. Comput. Chem.* **1996**, *17*, 1359–1370.
(34) Hariharan, P. C.; Pople, J. A. *Theor. Chim. Acta* **1973**, *28*, 213–222.
(35) Petersson, G. A.; Al-Laham, M. A. *J. Chem. Phys.* **1991**, *94*, 6081–6090.
(36) Petersson, G. A.; Bennett, A.; Tensfeldt, T. G.; Al-Laham, M. A.; Shirley, W. A.; Mantzaris, J. *J. Chem. Phys.* **1988**, *89*, 2193–2218.
(37) (a) Rassolov, V. A.; Pople, J. A.; Ratner, M. A.; Windus, T. L. *J. Chem. Phys.* **1998**, *109*, 1223–1229. (b) Wachters, A. J. H. *J. Chem. Phys.* **1970**, *52*, 1033. Bauschlicher, C. W., Jr.; Langhoff, S. R.; Barnes, L. A. *J. Chem. Phys.* **1989**, *91*, 2399.
(38) Becke, A. D. *J. Chem. Phys.* **1993**, *98*, 5648.
(39) Lee, C.; Yang, W.; Parr, R. G. *Phys. Rev. B* **1988**, *37*, 785.
(40) Clay, M. D.; Francis, E.; Jenney, J.; Hagedoorn, P. L.; George, G. N.; Adams, M. W. W.; Johnson, M. K. *J. Am. Chem. Soc.* **2002**, *124*, 788–805.
(41) Coelho, A. V.; Matias, P.; Fülöp, V.; Thompson, A.; Gonzalez, A.; Carrondo, M. A. *J. Biol. Inorg. Chem.* **1997**, *2*, 680–689.
(42) Santos-Silva, T.; Trincao, J.; Carvalho, A. L.; Bonifacio, C.; Auchere, F.; Raleiras, P.; Moura, I.; Moura, J. J.; Romao, M. J. *J. Biol. Inorg. Chem.* **2006**, *11*, 548–558.
(43) Katona, G.; Carpentier, P.; Nivière, V.; Amara, P.; Adam, V.; Ohana, J.; Tsanov, N.; Bourgeois, D. *Science* **2007**, *316*, 449–453.

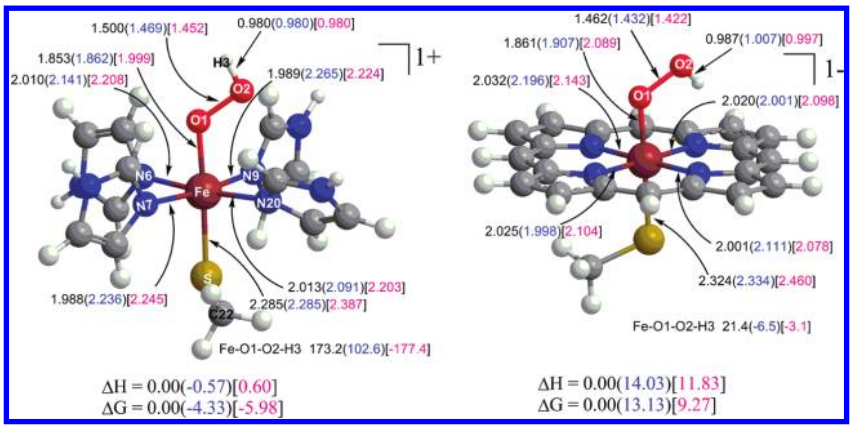

Figure 1. Ferric hydroperoxo model, $(SCH_3)(L)Fe^{III}-OOH$, for SOR (L = ImH_4) and P450 (L = Por). Enthalpies and free energies relative to the doublet state in kcal/mol, selected bond distances in Å, and selected dihedral angles in deg are presented for doublet, quartet (in parentheses), and sextet (in brackets) states.

sextet state match best with the experimentally-determined Fe−N distances. The high-spin structures have Fe−O and Fe−S bonds in a good agreement with the crystal structure, but these bonds are predicted to be too short in the lower spin states. Although, the N7−Fe−S−C22 dihedral angle is negative for the high-spin structure, in which the methyl group of methyl thiolate is on the opposite side of N7−Fe−S plane from the one found in the crystal structure, this angle is still near zero. The Fe−S−C22 and Fe−O1−C45 bond angles also vary from the crystal structure mainly because the interactions from the amino acid side chains are not included. In general, the all-electron basis set (BS-II) and the basis set with effective core potential on iron (BS-I) give similar structural parameters and the same trend for the relative free energies (Table 1). As expected from other studies,[44,45] the pure density functional, PBE, tends to prefer the low-spin states. With the B3LYP functional, the high-spin state has the lowest relative free energy, consistent with the experimental results. However, the high-spin geometries from PBE and B3LYP are not significantly different; the bond distances differ by only 0.01 Å, and the bond angles vary by 9°. Moreover, the calculated single-point energy by B3LYP with PBE optimized geometry gives the same trend for the relative free energies as B3LYP optimized geometry with high-spin state as the most stable structure. Therefore, we will apply B3LYP//PBE/BS-I to all other structures as this compromise produces the correct spin states and has more rapid geometry optimization than B3LYP.

Ferric Hydroperoxo Model, $(SCH_3)(L)Fe^{III}-OOH$. The ferric hydroperoxo, $Fe^{III}-OOH$, is a common intermediate observed at the active sites of both SOR and P450 enzymes. The optimized geometric parameters, enthalpies, and free energies relative to the low-spin state for the $(SCH_3)(L)Fe^{III}-OOH$ model of SOR and P450 active sites are shown in Figure 1. Mulliken atomic charges (all-electron basis sets give Fe charges as positive, but with similar trends; see Supporting Information), and spin densities are presented in Table 2. From the calculated spin densities, one and three unpaired electrons, for doublet and quartet states, respectively, reside mainly on the iron center in both enzyme models (>80%).

Table 2. Mulliken Atomic Charges and Spin Densities in Ferric Hydroperoxo Model, $(SCH_3)(L)Fe^{III}-OOH$ (L = ImH_4 for SOR and Por for P450)

	SOR			P450		
spin	1/2	3/2	5/2	1/2	3/2	5/2
total charge	1+	1+	1+	1−	1−	1−
			atomic charge			
Fe	−1.302	−1.107	−1.265	−1.169	−1.158	−1.209
O_p	−0.237	−0.442	−0.334	−0.075	−0.059	0.059
O_d	−0.543	−0.230	−0.411	−0.451	−0.472	−0.481
SCH_3	0.106	0.165	0.139	−0.017	0.018	−0.070
L	2.581	2.328	2.487	0.346	0.230	0.283
			atomic spin density			
Fe	0.869	3.063	4.035	0.880	2.804	4.011
O_p	0.103	0.006	0.245	0.154	0.176	0.408
O_d	0.007	−0.023	0.038	0.018	0.045	0.103
SCH_3	0.093	−0.112	0.452	0.050	0.001	0.300
L	−0.071	0.064	0.229	−0.102	−0.025	0.182

In the sextet state, four of the five unpaired electrons are on iron while the other is distributed somewhat differently in SOR and P450 models. In the SOR model, the other electron is mainly on the SCH_3 group (~45%) with the remainder split between the proximal oxygen (~25%) and the four imidazole ligands (~23%); in the P450 model, there is less on SCH_3 (~30%), more on the proximal oxygen (~41%), with the remainder distributed between the distal oxygen (~10%) and the porphyrin (~18%).

From the free energy calculations, SOR is predicted to have a high-spin ground state with low-spin and intermediate-spin states higher by 5.98 and 1.65 kcal/mol, respectively, whereas P450 is predicted to have a low-spin ground state with intermediate-spin and high-spin states higher by 13.13 and 9.27 kcal/mol, respectively (Figure 1). The high-spin ground state predicted for the SOR and the low-spin ground state predicted for the P450 model complexes, $(SCH_3)(L)Fe^{III}-OOH$, corresponds to that found experimentally.[46] Previous calculations for SOR

(44) Ghosh, A. *J. Biol. Inorg. Chem.* **2006**, *11*, 712–724.
(45) Swart, M.; Groenhof, A. R.; Ehlers, A. W.; Lammertsma, K. *J. Phys. Chem. A* **2004**, *108*, 5479–5483.
(46) (a) Mathe, C.; Mattioli, T. A.; Horner, O.; Lombard, M.; Latour, J.-M.; Fontecave, M.; Niviere, V. *J. Am. Chem. Soc.* **2002**, *124*, 4966. (b) Davydov, R.; Makris, T. M.; Kofman, V.; Werst, D. E.; Sligar, S. G.; Hoffman, B. M. *J. Am. Chem. Soc.* **2001**, *123*, 1403–1415.

Scheme 4. Molecular Orbital Energies (ε) of Selected High Energy Orbitals Relative to the Orbital of π-OOH^- Bonding to d_{xz} for the High-Spin $(SCH_3)(L)Fe^{III}-OOH$ Model for SOR; P450 Active Sites are Shown in Hartree for Both α and β Orbitals[a]

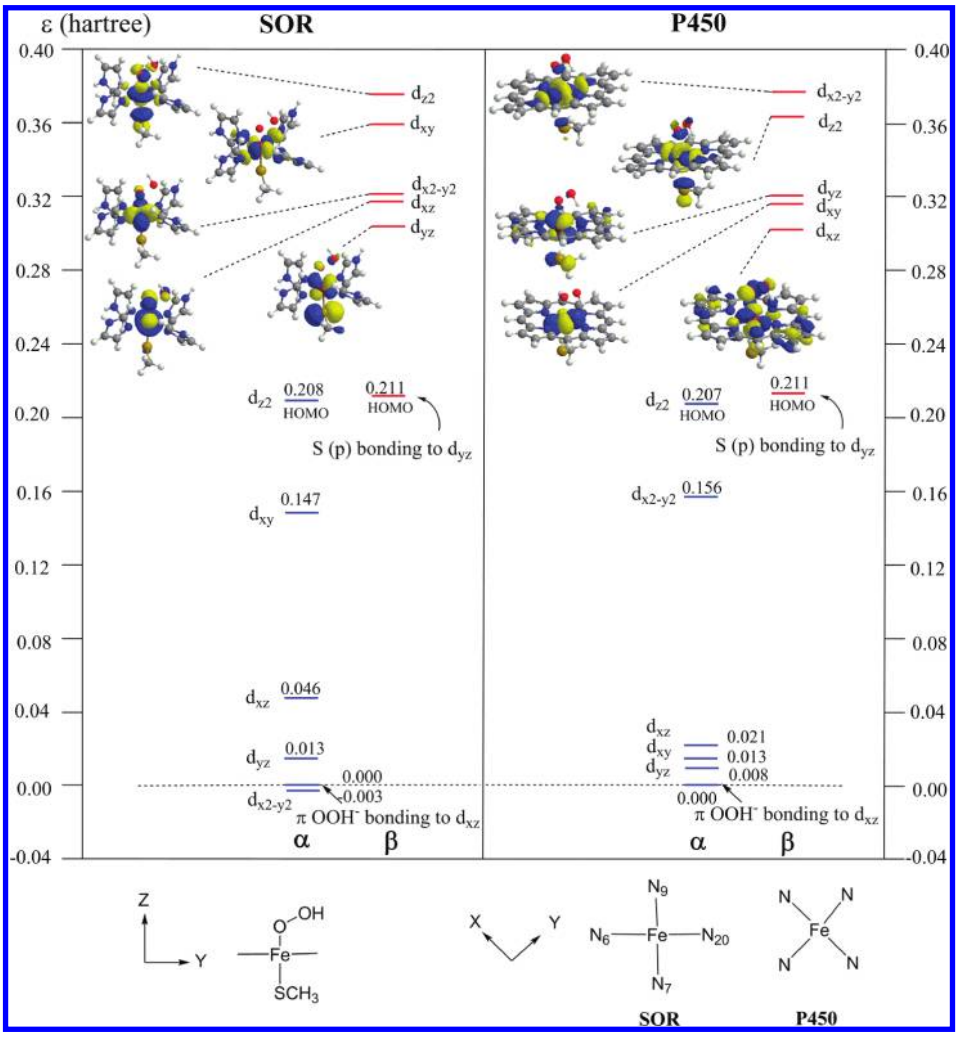

[a] Only the occupied (α spin) iron orbitals are shown. The absolute molecular orbital energies are $\varepsilon - 0.510$ for the SOR model and $\varepsilon - 0.262$ for the P450 model. Note that we defined the z-axis parallel to Fe−S bond and the y-axis parallel to O−O bond.

active site models have predicted both high-spin[28] and low-spin ground states.[26]

The difference in ground spin state for $Fe^{III}-OOH$ intermediates of P450 and SOR models derives from the difference in equatorial ligand structure, the constrained Fe−N bonds of the porphyrin ligand versus the extendable Fe−N bonds of imidazole ligands, which is reflected by their molecular orbital energies. Since the SOR and P450 models contain different total charges (1+ and 1−, respectively), one must scale the molecular orbital (MO) energies in order to make a comparison. Scheme 4 compares the MO energy levels for two enzyme models in the high-spin $(SCH_3)(L)Fe^{III}-OOH$ complexes. Here, all five singly occupied MOs consist mainly of iron d-orbital contributions antibonding to ligand orbitals. Since we defined the y-axis to be parallel to the O−O bond and the orientation of O−O bond over the equatorial ligand plane is different in the SOR and P450 models as shown Scheme 4, $d_{x^2-y^2}$ in the P450 model and d_{xy} in the SOR model are σ-antibonding to the equatorial ligands, whereas d_{xy} in the P450 model and $d_{x^2-y^2}$ in the SOR model are π-antibonding to the equatorial ligands. In the high-spin state, unlike low- and intermediate-spin states, unpaired electrons occupy $d_{x^2-y^2}$ and d_{z^2} orbitals, which are σ-antibonding to ligand orbitals; lengthening of the Fe−N, Fe−O, and Fe−S bonds stabilizes these orbitals. The MO energies of $d_{x^2-y^2}$ orbital in the P450 model are higher than the d_{xy} orbital in the SOR model. With no ligand constraints, all Fe−O, Fe−S, and Fe−N bond distances in the sextet state of the SOR model are longer than the corresponding ones in doublet and quartet states (Figure 1). However, for the P450 model, although the Fe−O and Fe−S bond distances in the sextet state are longer than the ones in the doublet and quartet states, the porphyrin constrains the Fe−N bond distances such that they are unchanged for different spin states. Therefore, the constrained ring of porphyrin ligand disfavors the high-spin ground state of $(SCH_3)(L)Fe^{III}-OOH$ for the P450 model, whereas the more extendable Fe−N bonds of the imidazole ligands accommodate the high-spin ground state in the SOR model.

The different ground spin states of $(SCH_3)(L)Fe^{III}-OOH$ intermediates for SOR and P450 models can contribute to different reaction paths. Interestingly, the

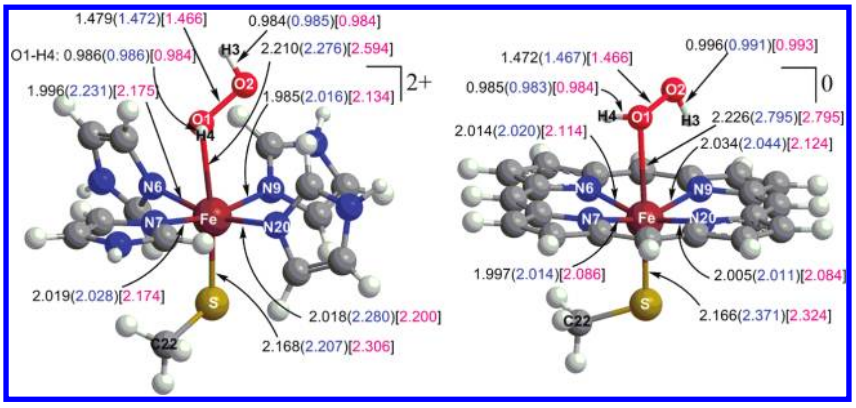

Figure 2. Ferric hydrogen peroxide model, $(SCH_3)(L)Fe^{III}-HOOH$, for SOR (L = ImH_4) and P450 (L = Por). The selected bond distances in Å are presented for doublet, quartet (in parentheses), and sextet (in brackets) states.

higher spin states for both enzyme models have shorter O−O bond distances and longer Fe−O bond distances (Figure 1). Thus, the high-spin ground state in SOR has a strong O−O bond but a weak Fe−O bond, whereas the low-spin ground state in P450 has a weak O−O bond but a strong Fe−O bond. Moreover, in SOR, the atomic charge (Table 2) on the distal oxygen in the high-spin ground state is only slightly more negative than that on the proximal oxygen (−0.411 and −0.334, respectively), whereas the atomic charge on the distal oxygen in its low-spin state is much more negative than that on the proximal oxygen (−0.543 and −0.237, respectively). The same situation is found for the low-spin ground state in P450; the atomic charge on the distal oxygen is highly negative (−0.481) in comparison to that on proximal oxygen, which is almost neutral (0.059). Therefore, the charges and the distances in the high-spin $(SCH_3)(L)Fe^{III}-OOH$ models, as found for SOR, favor protonation at proximal oxygen and Fe−O bond cleavage, whereas the charges and the distances in the low-spin $(SCH_3)(L)Fe^{III}-OOH$ models, as found for P450, favor protonation at distal oxygen and O−O bond cleavage. Previous studies of other ferric hydroperoxo[47] and alkylperoxo[48,49] complexes also support the Fe−O bond cleavage for the high-spin complex and O−O bond cleavage for the low-spin complex.

Ferric Hydrogen Peroxide Model, $(SCH_3)(L)Fe^{III}-HOOH$, versus Oxo-Ferryl Model, $(SCH_3)(L)Fe^{IV}=O$. The protonation at the proximal oxygen of ferric hydroperoxo, $Fe^{III}-OOH$, leads to the formation of ferric hydrogen peroxide ($Fe^{III}-HOOH$), the intermediate prior to Fe−O bond cleavage and release of H_2O_2, the product of SOR catalytic cycle. For both SOR and P450 models, in comparison to $(SCH_3)(L)Fe^{III}-OOH$, the $(SCH_3)(L)Fe^{III}-HOOH$ has a shorter Fe−S bond and a longer Fe−O bond in preparation for H_2O_2 release (Figures 1 and 2). For the SOR model, the sextet ground state of $(SCH_3)(L)Fe^{III}-HOOH$ is much lower in free energy than the doublet and quartet states, which have free energies close to each other (Table 3). For the P450 model, the high-spin state of $(SCH_3)(L)Fe^{III}-HOOH$ is found to lie very close in free energy to low- and intermediate-spin states, all within a range of 1 kcal/mol (Table 3). Like $(SCH_3)(L)Fe^{III}-OOH$,

Table 3. Relative Enthalpies and Free Energies (kcal/mol) of Ferric Hydrogen Peroxide and Oxo-Ferryl Models with Respect to the Doublet State of $(SCH_3)(L)Fe^{III}-HOOH$ (L = ImH_4 for SOR and Por for P450)

	spin	ΔH	ΔG
SOR			
$[(SCH_3)(ImH)_4Fe^{III}-HOOH]^{2+}$	$S = 1/2$	0.00	0.00
	$S = 3/2$	0.74	−2.65
	$S = 5/2$	−7.06	−13.47
$[(SCH_3)(ImH)_4Fe^{IV}=O]^{2+} + H_2O$	$S = 1/2$	−7.59	−18.69
	$S = 3/2$	−8.76	−20.33
	$S = 5/2$	−4.09	−19.17
$[(SCH_3)(ImH)_4Fe^{IV}=O\cdots H_2O]^{2+}$	$S = 1/2$	−16.38	−19.58
	$S = 3/2$	−16.45	−18.66
	$S = 5/2$	−10.19	−16.58
P450			
$[(SCH_3)(Por)Fe^{III}-HOOH]^{0}$	$S = 1/2$	0.00	0.00
	$S = 3/2$	4.78	1.09
	$S = 5/2$	3.45	−0.17
$[(SCH_3)(Por)Fe^{IV}=O]^{0} + H_2O$	$S = 1/2$	−3.99	−14.66
	$S = 3/2$	−5.37	−16.80
	$S = 5/2$	6.87	−5.11
$[(SCH_3)(Por)Fe^{IV}=O\cdots H_2O]^{0}$	$S = 1/2$	−10.25	−12.76
	$S = 3/2$	−11.47	−14.46
	$S = 5/2$	0.93	−2.76

Table 4. Mulliken Atomic Charges and Spin Densities in Ferric Hydrogen Peroxide Model, $(SCH_3)(L)Fe^{III}$-HOOH (L = ImH_4 for SOR and Por for P450)

	SOR			P450		
spin	1/2	3/2	5/2	1/2	3/2	5/2
total charge	2+	2+	2+	0	0	0
	atomic charge					
Fe	−1.423	−1.404	−1.389	−1.181	−0.965	−1.092
O_p	−0.080	−0.069	−0.159	0.155	−0.010	0.026
O_d	−0.465	−0.449	−0.441	−0.555	−0.550	−0.573
SCH_3	0.459	0.531	0.531	0.317	0.150	0.325
L	2.722	2.588	2.665	0.487	0.639	0.563
	atomic spin density					
Fe	0.879	3.154	3.997	0.968	2.582	4.042
O_p	−0.007	−0.012	−0.026	−0.010	−0.025	−0.018
O_d	0.000	0.000	0.006	0.000	0.007	0.005
SCH_3	0.195	−0.187	0.783	0.129	0.534	0.559
L	−0.066	0.044	0.242	−0.088	−0.090	0.420

(47) Lehnert, N.; Neese, F.; Ho, R. Y. N.; Lawrence Que, J.; Solomon, E. I. *J. Am. Chem. Soc.* **2002**, *124*, 10810–10822.
(48) Lehnert, N.; Ho, R. Y. N.; Que, L.; Solomon, E. I. *J. Am. Chem. Soc.* **2001**, *123*, 12802–12816.
(49) Lehnert, N.; Ho, R. Y. N.; Que, L.; Solomon, E. I. *J. Am. Chem. Soc.* **2001**, *123*, 8271–8290.

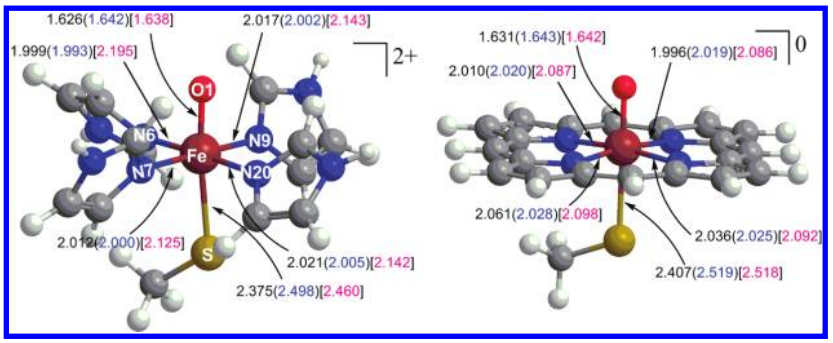

Figure 3. Oxo-ferryl model, $(SCH_3)(L)(Fe^{IV}) = O + H_2O$, for SOR (L = ImH_4) and P450 (L = Por). The selected bond distances in Å are presented for doublet, quartet (in parentheses), and sextet (in brackets) states.

the calculated spin density predicts that the one and three unpaired electrons for doublet and quartet states of $(SCH_3)(L)Fe^{III}-HOOH$ reside mainly on the iron center (Table 4). For the sextet state, four of five unpaired electrons are on iron while the other unpaired electron is distributed mainly on SCH_3 (~78%) with the remainder on four imidazole ligands (~24%) in the SOR model but distributed between both SCH_3 (~56%) and porphyrin (~42%) in the P450 model. Unlike $(SCH_3)(L)Fe^{III}-OOH$, the proximal oxygen in $(SCH_3)(L)Fe^{III}-HOOH$ has very low spin density due to the long Fe−O bond. In both enzyme models, a low spin density is found on the distal oxygen in $(SCH_3)(L)Fe^{III}-HOOH$ (Table 4) as in $(SCH_3)(L)Fe^{III}-OOH$ (Table 1).

Protonation at the distal oxygen of ferric hydroperoxo leads to O−O bond cleavage and formation of the oxo-ferryl complex, $Fe^{IV}=O$, and H_2O, the main product for P450. The $(SCH_3)(L)Fe^{IV}=O$ model complexes are calculated for both P450 and SOR (Figure 3) to compare their stability with that of $(SCH_3)(L)Fe^{III}-HOOH$. In both SOR and P450 models, $(SCH_3)(L)Fe^{IV}=O$ has a much shorter Fe−O bond and a longer Fe−S bond than those in $(SCH_3)(L)Fe^{III}-OOH$, implying a strong Fe−O bond with stronger trans influence. Unlike either $(SCH_3)(L)Fe^{III}-OOH$ or $(SCH_3)(L)Fe^{III}-HOOH$, the spin density calculations for both doublet and quartet spin states of $(SCH_3)(L)Fe^{IV}=O$ for both enzyme models (Table 5) show two unpaired electrons of the same spin distributed more or less equally over both the iron and oxygen atoms,[14] whereas the third unpaired electron is distributed on SCH_3 and the equatorial ligands, antiparallel and parallel to the other two unpaired electrons, respectively. Although, in both SOR and P450 models, the third unpaired electron is mainly on SCH_3 with less on the equatorial ligand, there is a greater amount of spin density on porphyrin compare to a minor amount on four imidazole ligands because of the conjugated structure of the porphyrin in P450. Moreover, the issue of whether the spin density distribution from the third unpaired electron is mainly on sulfur or porphyrin can depend on various aspects of the model[14,50] and is particularly sensitive to H bonding to the thiolate.[28,51,52] Further, the energetic differences between these different spin distributions are small.

Table 5. Mulliken Atomic Charges and Spin Densities in Oxo-Ferryl Model, $(SCH_3)(L)Fe^{IV}=O$ (L = ImH_4 for SOR and Por for P450)

	SOR			P450		
spin	1/2	3/2	5/2	1/2	3/2	5/2
total charge	2+	2+	2+	0	0	0
			atomic charge			
Fe	−0.812	−0.738	−0.768	−0.724	−0.626	−0.600
O_p	−0.518	−0.495	−0.505	−0.381	−0.369	−0.395
SCH_3	0.509	0.420	0.493	0.296	0.220	0.250
L	2.821	2.813	2.781	0.809	0.775	0.745
			atomic spin density			
Fe	1.157	1.106	3.053	1.177	1.093	3.087
O_p	0.965	0.940	0.722	0.937	0.950	0.707
SCH_3	−1.000	0.938	0.851	−0.726	0.687	0.581
L	−0.123	0.015	0.374	−0.388	0.270	0.626

In the SOR model, the quartet ground state of $(SCH_3)(L)Fe^{IV}=O$ is found to lie close to the sextet and doublet states, which have free energies within ~1 kcal/mol (Table 3). In the P450 model, the ground state of the $(SCH_3)(L)Fe^{IV}=O$ complex is also the quartet state, which has free energy close to the doublet state but much lower than the sextet state. Considering the relative free energies for the various states of both $(SCH_3)(L)Fe^{III}-HOOH$ and $(SCH_3)(L)Fe^{IV}=O + H_2O$ (Table 3), the most stable structure is the $(SCH_3)(L)Fe^{IV}=O$ complex in the quartet state for both SOR and P450 models. The low free energy of the $(SCH_3)(L)Fe^{IV}=O$ complexes and H_2O in comparison to the $(SCH_3)(L)Fe^{III}-HOOH$ complexes is largely derived from the entropy contribution (~−11 to −15 kcal/mol), which favors $(SCH_3)(L)-Fe^{IV}=O$ and H_2O, the dissociated products, over $(SCH_3)(L)Fe^{III}-HOOH$, a single product. In the P450 model, the free energy of the quartet state of $(SCH_3)-(L)Fe^{IV}=O$ and H_2O is much more favorable than that of the sextet state of $(SCH_3)(L)Fe^{III}-HOOH$ by −16.63 kcal/mol, whereas the enthalpy change favors the quartet state $(SCH_3)(L)Fe^{IV}=O$ and H_2O by a smaller number (−8.82 kcal/mol). In the SOR model, the enthalpy of the sextet ground state of $(SCH_3)(L)Fe^{III}-HOOH$ is only 1.60 kcal/mol higher than the enthalpy of the quartet ground state of $(SCH_3)(L)Fe^{IV}=O$ and H_2O, whereas the free energy difference is 6.86 kcal/mol.

To ensure that the lower free energy of the $(SCH_3)-(L)Fe^{IV}=O$ complex compared to the $Fe^{III}-HOOH$ complex in both enzyme active site models is not entirely from the dissociation of H_2O, we also calculated

(50) Ogliaro, F.; Cohen, S.; Filatov, M.; Harris, N.; Shaik, S. *Angew. Chem., Int. Ed.* **2000**, *39*, 3851–3855.
(51) Ogliaro, F.; Cohen, S.; Visser, S. P. d.; Shaik, S. *J. Am. Chem. Soc.* **2000**, *122*, 12892–12893.
(52) Schoneboom, J. C.; Lin, H.; Reuter, N.; Thiel, W.; Cohen, S.; Ogliaro, F.; Shaik, S. *J. Am. Chem. Soc.* **2002**, *124*, 8142–8151.

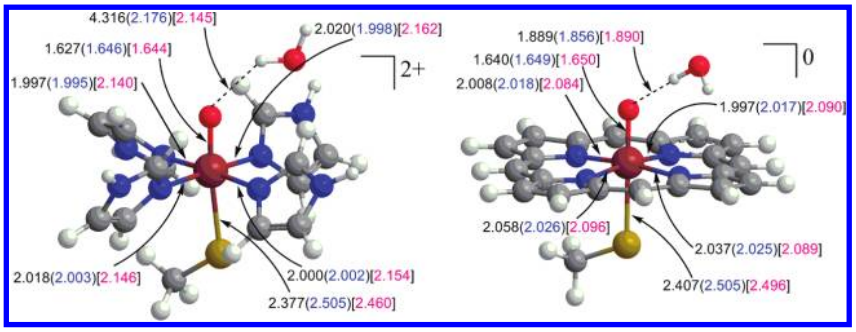

Figure 4. Oxo-ferryl model with a water molecule, $(SCH_3)(L)Fe^{IV}{=}O\cdots H_2O$, for SOR (L = ImH_4) and P450 (L = Por). The selected bond distances in Å are presented for doublet, quartet (in parentheses), and sextet (in brackets) states.

water-bound oxo-ferryl, $(SCH_3)(L)Fe^{IV}{=}O\cdots H_2O$, complex (Figure 4). Although the Fe−O bond is slightly longer in $(SCH_3)(L)Fe^{IV}{=}O\cdots H_2O$ than that in (SCH_3)-$(L)Fe^{IV}{=}O$, there is no significant change in the overall geometry. The relative free energies of $(SCH_3)(L)Fe^{IV}{=}O\cdots H_2O$ product show a similar trend to those of $(SCH_3)(L)Fe^{IV}{=}O$ and H_2O products (Table 3). For the P450 model, the doublet ground state of $(SCH_3)(L)Fe^{III}-OOH$ favors protonation at distal oxygen, which corresponds to the fact that the quartet ground state of $(SCH_3)(L)Fe^{IV}{=}O\cdots H_2O$ product is more favorable than the sextet ground state of $(SCH_3)(L)Fe^{III}-HOOH$ by 14.3 kcal/mol. This result is consistent with the appearance of Cpd I in the P450 catalytic cycle, in which the quartet ground state of the $(SCH_3)(L)Fe^{IV}{=}O$ complex is found with the free energy lying close to the doublet state as in previous computational studies.[14,53−55] On the other hand, for the SOR model, the doublet state of (SCH_3)-$(L)Fe^{IV}{=}O\cdots H_2O$ is the lowest free energy spin state with the quartet state lying very close. Although, in the SOR model, the electronic structure of the sextet ground state of $(SCH_3)(L)Fe^{III}-OOH$ could support the formation of the $(SCH_3)(L)Fe^{III}-HOOH$, the intermediate to produce H_2O_2, the sextet ground state $(SCH_3)(L)Fe^{III}-HOOH$ is still lying 6.11 kcal/mol higher than the doublet ground state $(SCH_3)(L)Fe^{IV}{=}O\cdots H_2O$. Although there is a real trend toward P450 favoring the oxo-ferryl species more than SOR, there must be other factors that stabilize the $Fe^{III}-HOOH$ intermediate or favor its production in SOR. Here, it is important to note that only the relative energies are trustworthy, so the calculations, even for these simple models, predict the correct experimental trends. In the next section, the effect of hydrogen bonding from explicit water molecules will be included to represent the solvent-exposed location of the active site of SOR.

Models Including Explicit Water Molecules for Ferric Hydrogen Peroxide, $(SCH_3)(L)Fe^{III}-HOOH\cdots 2H_2O$, and Oxo-Ferryl, $(SCH_3)(L)Fe^{IV}{=}O\cdots 3H_2O$. Since the active site of SOR is located at a solvent-exposed position, hydrogen bonding between the iron-bound H_2O_2 and water molecules could be involved in stabilizing the $Fe^{III}-HOOH$ species. On the other hand, the active site of P450 is located within an enclosed pocket of the enzyme and this may limit the number of water molecules near the enzyme active site.[13] However, in this examination of the effects of explicit H_2O molecules, we will assume a similar arrangement of H_2O molecules for the $(SCH_3)(L)Fe^{III}-HOOH$ model of both SOR and P450. The free energy of the $(SCH_3)(L)Fe^{III}-HOOH\cdots 2H_2O$ complex, in which two water molecules and the proximal and distal oxygen atoms form three hydrogen bonds, is calculated and compared to the free energy of the $(SCH_3)(L)Fe^{IV}{=}O$ complex and three-water-molecule cluster and the free energy of the $(SCH_3)(L)$-$Fe^{IV}{=}O\cdots 3H_2O$ complex. This latter complex and three-water-molecule cluster are chosen to provide the same total number of hydrogen bonds in order to provide a fair energetic comparison. The relative free energies and enthalpies of $(SCH_3)(L)Fe^{III}-HOOH\cdots 2H_2O$, $(SCH_3)(L)Fe^{IV}{=}O$ + $3H_2O$ cluster, and $(SCH_3)(L)$-$Fe^{IV}{=}O\cdots 3H_2O$ active site models of SOR and P450, which included three hydrogen bonds from explicit water molecules, are shown in Table 6.

Table 6. Relative Enthalpies and Free Energies (kcal/mol) of Ferric Hydrogen Peroxide and Oxo-Ferryl Models with Two Extra Water Molecules with Respect to the Doublet State of $(SCH_3)(L)Fe^{m}-HOOH\cdots 2H_2O$ (L = ImH_4 for SOR and Por for P450)

	spin	ΔH	ΔG
SOR			
$[(SCH_3)(ImH)_4Fe^{III}-HOOH\cdots 2H_2O]^{2+}$	$S = 1/2$	0.00	0.00
	$S = 3/2$	0.66	−2.66
	$S = 5/2$	−5.23	−10.84
$[(SCH_3)(ImH)_4Fe^{IV}{=}O]^{2+}$ + $3H_2O$ cluster	$S = 1/2$	5.83	−6.06
	$S = 3/2$	4.66	−7.71
	$S = 5/2$	9.33	−6.55
$[(SCH_3)(ImH)_4Fe^{IV}{=}O\cdots 3H_2O]^{2+}$ Model-1	$S = 1/2^a$	−4.36	−8.18
	$S = 3/2^a$	−4.41	−8.70
	$S = 5/2^a$	1.67	−4.86
$[(SCH_3)(ImH)_4Fe^{IV}{=}O\cdots 3H_2O]^{2+}$ Model-2	$S = 1/2^b$		
	$S = 3/2^a$	−9.90	−10.68
	$S = 5/2$	−1.55	−8.91
P450			
$[(SCH_3)(Por)Fe^{III}-HOOH\cdots 2H_2O]^0$	$S = 1/2$	0.00	0.00
	$S = 3/2$	4.10	1.39
	$S = 5/2$	0.89	−2.31
$[(SCH_3)(Por)Fe^{IV}{=}O]^0$ + $3H_2O$ cluster	$S = 1/2$	−6.66	−17.66
	$S = 3/2$	−8.05	−19.80
	$S = 5/2$	4.20	−8.11
$[(SCH_3)(Por)Fe^{IV}{=}O\cdots 3H_2O]^0$	$S = 1/2$	−17.87	−18.43
	$S = 3/2$	−18.71	−20.07
	$S = 5/2$	−5.97	−7.77

[a] Structures have one small imaginary frequency (∼ −30). [b] Water cluster dissociates from Fe=O complex.

(53) Altun, A.; Shaik, S.; Thiel, W. *J. Am. Chem. Soc.* **2007**, *129*, 8978–8987.
(54) Ogliaro, F. o.; Filatov, M.; Shaik, S. *Eur. J. Inorg. Chem.* **2000**, 2455–2458.
(55) Liu, X.; Wang, Y.; Han, K. *J. Biol. Inorg. Chem.* **2007**, *12*, 1073–1081.

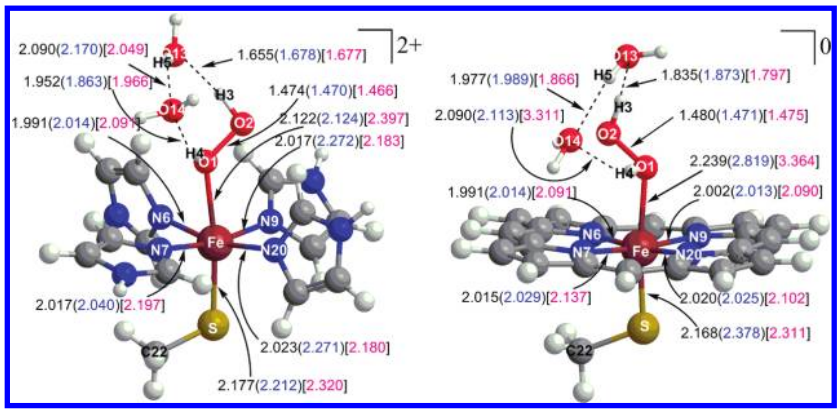

Figure 5. Ferric hydrogen peroxide model with hydrogen bonding from two explicit water molecules, $(SCH_3)(L)Fe^{III}-HOOH\cdots 2H_2O$, for SOR (L = ImH_4) and P450 (L = Por). The selected bond distances in Å are presented for doublet, quartet (in parentheses), and sextet (in brackets) states.

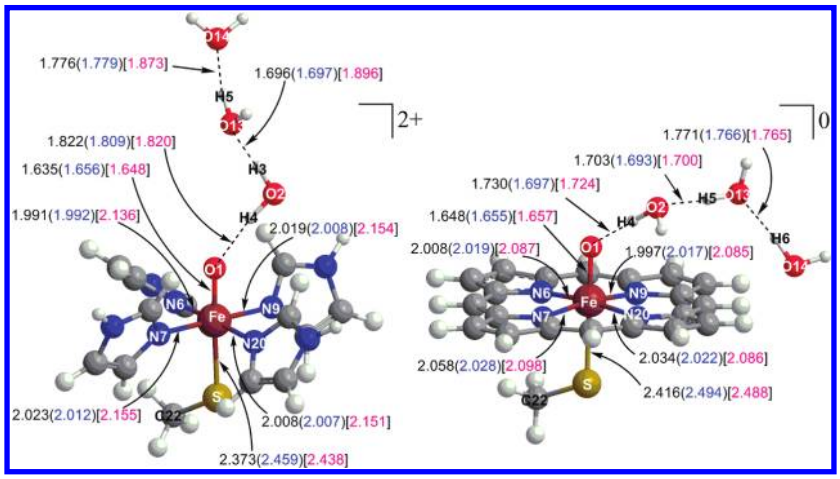

Figure 6. Oxo-ferryl model with hydrogen bonding from three explicit water molecules, $(SCH_3)(L)Fe^{IV}=O\cdots 3H_2O$, for SOR (L = ImH_4) Model-1 and P450 (L = Por). The selected bond distances in Å are presented for doublet, quartet (in parentheses), and sextet (in brackets) states.

The addition of two water molecules to the $(SCH_3)(L)Fe^{III}-HOOH$ model creates three hydrogen bonds: O14−H4, O14−H5, and O13−H3 (Figure 5); $(SCH_3)(L)Fe^{IV}=O\cdots 3H_2O$ also has three hydrogen bonds: O1−H4, O13−H3, and O14−H5 (Figure 6), as does $(SCH_3)(L)Fe^{IV}=O$ and three-water-molecule cluster (Figure 7). Initially, for the SOR model, the fully optimized structure of $(SCH_3)(L)Fe^{IV}=O\cdots 3H_2O$ had four hydrogen bonds, where the fourth hydrogen bond was formed between O14 and N−H from one of the imidazole ligands. Therefore, to keep the water chain in the upright direction, preventing the formation of the fourth H bond in $(SCH_3)(L)Fe^{IV}=O\cdots 3H_2O$ for the SOR model, we calculated two other structures: (1) Model-1 which has the bond angles of Fe−O1−H4, O1−H4−O2, and O2−H3−O13 fixed (Figure 6) during the geometry optimization; and (2) Model-2 which has dihedral angle Fe−O1−O2−O13 fixed at 180°. Since both models gave similar relative energies in comparison to the $(SCH_3)(L)Fe^{III}-HOOH\cdots 2H_2O$ complex (Table 6), the $(SCH_3)(L)Fe^{IV}=O\cdots 3H_2O$ model for SOR that will be discussed from here is referred to as $(SCH_3)(L)Fe^{IV}=O\cdots 3H_2O$ Model-1.

For both SOR and P450 models, the iron−ligand bond lengths of $(SCH_3)(L)Fe^{IV}=O\cdots 3H_2O$ are not significantly changed from $(SCH_3)(L)Fe^{IV}=O$. The relative free energies of $(SCH_3)(L)Fe^{IV}=O\cdots 3H_2O$ and $(SCH_3)(L)Fe^{IV}=O + 3H_2O$ cluster show similar trends (Table 6) for the P450 model; the quartet ground state lies close to the doublet state, and the sextet state has higher free energy. For the SOR model, all spin states have similar energies for $(SCH_3)(L)Fe^{IV}=O + 3H_2O$ cluster, whereas the doublet and quartet states in the $(SCH_3)(L)Fe^{IV}=O\cdots 3H_2O$ model have lower free energy than the sextet state by ∼−4 kcal/mol.

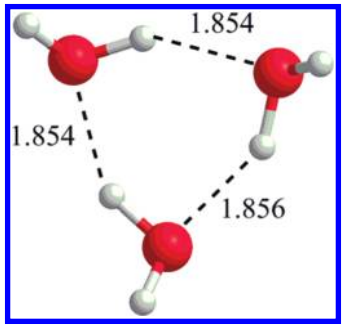

Figure 7. Optimized three water cluster containing three H---O hydrogen bonds. Selected distances are given in Å. The cluster was optimized using BS-II.

With two explicit water molecules, the Fe−O bond in the P450 model of $(SCH_3)(L)Fe^{III}-HOOH\cdots 2H_2O$ lengthens from that without water molecules (Figures 2 and 5).

Clearly, the hydrogen bonds from water molecules do not help to stabilize $(SCH_3)(L)Fe^{III}-HOOH$ in the P450 model; the quartet ground state of both the $(SCH_3)(L)Fe^{IV}=O\cdots 3H_2O$ complex and the $(SCH_3)(L)Fe^{IV}=O + 3H_2O$ cluster still have lower free energies than the sextet ground state of $Fe^{III}-HOOH\cdots 2H_2O$ by >-18 kcal/mol (Table 6). Unlike the P450 model, the SOR model of $(SCH_3)(L)Fe^{III}-HOOH\cdots 2H_2O$ has a shorter Fe−O bond than that without explicit water molecules by 0.1−0.2 Å (Figures 2 and 5). The hydrogen bonds from water molecules in the SOR model stabilize $(SCH_3)(L)Fe^{III}-HOOH$ as reflected in the stronger Fe−O bond. With hydrogen bonds from just water molecules, the sextet ground state of $(SCH_3)(L)Fe^{III}-HOOH\cdots 2H_2O$ is now more stable than the quartet ground state of either the $(SCH_3)(L)Fe^{IV}=O\cdots 3H_2O$ complex or the $(SCH_3)(L)Fe^{IV}=O + 3H_2O$ cluster by −2.14 and −3.13 kcal/mol in free energy, respectively. Our result suggests that the solvent-exposed position of the active site in the SOR enzyme is a significant factor that stabilizes the ferric hydrogen peroxide complex and leads SOR to hydrogen peroxide production rather than oxo-ferryl formation. As mentioned above, only the relative energies are trustworthy; thus, it would be incorrect for the reader to conclude that these calculations actually predict that SOR might have some oxy-ferryl activity. The calculations predict that SOR will have less oxy-ferryl activity and more H_2O_2 production than P450.

Conclusions

The different ground spin states of the $Fe^{III}-OOH$ intermediates in the SOR and P450 enzymes lead these two intermediates along different reaction pathways. For both P450 and SOR models, we compute that the lower spin states have shorter Fe−O bonds, longer O−O bonds, and more negative charge on the proximal oxygen than on the distal oxygen when compared to the higher spin intermediates. Therefore, for both systems, we find that a lower spin iron center favors protonation of the distal oxygen, release of H_2O, and production of a high-valent $Fe^{IV}=O$ ferryl oxide species, while a higher spin iron center favors protonation of the proximal oxygen atom and loss of H_2O_2. We show that these two different ligand sets have a marked effect on the nature of the ground spin state of these Fe^{III} systems. For the P450 models, in which the porphine ligand constrains the Fe−N distances, we compute a low-spin singlet ground state for the $Fe^{III}-OOH$ intermediate. Therefore, we would expect this species to undergo protonation at the distal oxygen atom and O−O bond cleavage to yield H_2O and the ferryl oxide complex $Fe^{IV}=O$ from this system. For the SOR models, in which the Fe−N distances are not constrained, we compute a high-spin sextet ground state for the $Fe^{III}-OOH$ intermediate. Therefore, we would expect protonation of the proximal oxygen atom and dissociation of H_2O_2 from the SOR system.

Another factor that effects which product is formed is the active site locations in the respective enzymes. The P450 active site is located on the inside of the P450 enzyme and, thus, has limited access to the aqueous solvent, while the SOR active site is located on the surface of the SOR enzyme and, thus, has direct access to the aqueous solvent. We modeled the effects of solvation on these enzyme active sites by including two water molecules in our models. The presence of water molecules near these enzyme active sites was found to affect the course of these reactions in two complementary ways. The addition of these water molecules, which act as hydrogen bond donors to the iron-bound H_2O_2, (1) stabilizes higher spin states of the Fe^{III} center and (2) weakens the Fe−O interaction between H_2O_2 and the Fe^{III} center. These computations show that the addition of H_2O solvent favors H_2O_2 formation over O−O cleavage.

Although these computations due not assess the kinetics of these reactions, the solvent exposed site in SOR may also provide a kinetic lability for the dissociation of the H_2O_2 from the enzyme active site. Our calculations show that the thermodynamics of the reaction path is controlled by two factors: the spin state from the differences between the four N-donor ligands in P450 versus SOR and the degree of solvent-exposure from the location of the active site.

Acknowledgment. We would like to thank the National Science Foundation (Grant Nos. CHE-0518074, CHE-0541587, and CHE-0910552), the Welch Foundation (Grant No. A-0648), and Royal Thai Government for financial support.

Supporting Information Available: Four tables (S1−S4) reporting Mulliken charges, spin densities, and energies for the calculations in BS-III. This material is available free of charge via the Internet at http://pubs.acs.org.